RSC Advances




ROYAL SOCIETY OF CHEMISTRY

www.rsc.org/advances

# Fabrication and analysis of dye-sensitized solar cells (DSSCs) using porphyrin dyes with catechol anchoring group

Maryam Adineh[a], Pooya Tahay[a], Mohsen Ameri[b], , Nasser Safari[a*],Ezeddin Mohajerani[c]

*a Department of Chemistry, Shahid Beheshti University, Evin, 1983963113 Tehran, Iran*

*bDepartment of Physics, Bu- Ali Sina University, Hamedan, Iran*

*c Laser and Plasma Research Institute, Shahid Beheshti University, Tehran, 1983969411, Iran*

E-mail: n-safari@sbu.ac.ir

**Abstract**

Herein, we report the preparation and application of 4 different Zinc(II) tetrakis(dihydroxyphenyl) porphyrin (ZnTDHPP) as the sensitizing dyes in dye sensitized solar cells (DSSCs). The experiment includes solution and solid state UV-Vis data, steady state current-voltage characteristics, and our theoretical analysis is comprised of density functional theory (DFT) and langmuir isotherm adsorption formalism. The results show that the Zn tetrakis(2, 3dihydroxyphenyl) porphyrin (Zn2, 3TDHPP) and Zn tetrakis(3, 4dihydroxyphenyl) porphyrin (Zn3, 4TDHPP) with adjacent hydroxyl groups attached to $TiO_2$ surface much stronger than carboxylate The catechol anchoring group showed high stability of the dye on the $TiO_2$ surface. The cells prepared by these porphyrins showed no significant desorption of dye from the $TiO_2$ surface after days. The DSSCs based on Zn2, 3TDHPP showed the best photovoltaic performance under AM 1.5 irradiation comparable to the conventional Zn tetrakis(p-carboxyphenyl) porphyrin(ZnTCPP), despite lower dye loading on $TiO_2$ surface.

However, non-cooperative OH bonding on $TiO_2$ for Zn2,4TDHPP and Zn2, 5TDHPP showed weak attachment to $TiO_2$ surface and lower efficiencies. DFT calculations showed that Zn2,3TDHPP structure is more nonplanar than the others that may suppress dye aggregation. The adopted adsorption modeling is fitted to the experimental data to study the kinetics of dye loading. The study can be herald of developing new class of porphyrin sensitizers for DSSC applications.

.**Keywords:** dye sensitized solar cells, dihydroxyphenyl, anchoring group, catechol porphyrin

## 1 Introduction

With population increase, resource depletion and the rising cost of fossil energy sources, researchers have tried to develop clean and renewable energy such as solar energy. Solar energy is an abundant, renewable and clean energy sources that could supply energy for societies. Dye sensitized solar cells (DSSCs) are the third generation of solar cells which were first developed by O'Regan and Grätzel in 1991[1]. DSSC is generally comprised of a photoanode which is made of a semiconductor, sensitizer (dye molecules) on transparent conducting oxide (TCO) substrate and hole conducting material as electrolyte. Photo excitation of dye molecules leads to electron injection into the conduction band of the semiconductor metal oxide (generally titanium dioxide) which is in contact with an electrolyte solution, generating oxidized dye. The process is followed by electron transfer from the electrolyte to sensitizer and dye regeneration. [2-4]

Inspired by the important role of porphyrins in the photosynthesis, many researchers have used porphyrin derivatives as sensitizer in DSSCs [5-14]. Thus far, the highest DSSCs efficiency has been reported for a porphyrin dye[12]. Porphyrins are macrocyclic compounds with highly π-

conjugated systems exhibiting intense absorptions in the visible region. Some functional groups can extend porphyrin and increase their ability to absorb light, therefore making them good choices for use in solar energy conversion. Catechol is such functional group which could extend porphyrin π-system [15]. Catechol porphyrins have potential application in solar cells [16, 17]. Ortho dihydroxy phenyl functional groups in catechol porphyrins are directly at the meso positions. Ortho dihydroxy phenyl can easily be oxidized to orthoquinone by electrochemical methods [18]. Porphyrins and catechol are both active in electrochemistry, and putting together and coupling these two compounds could make new compounds with interesting properties [15-17, 19].

Anchoring groups play an important role in DSSCs. In order to have a fast electron injection into the $TiO_2$ semiconductor, the existence of anchoring groups is crucial to attach the dye on a $TiO_2$ surface. Carboxylic acid is an anchoring group which has been widely studied [20-25]. The major binding modes for the carboxylic acid anchoring groups are a bidentate chelating and/or a bidentate bridging of the carboxylate on the $TiO_2$ surface but an unidentate mode is also possible (chart 1) [26].

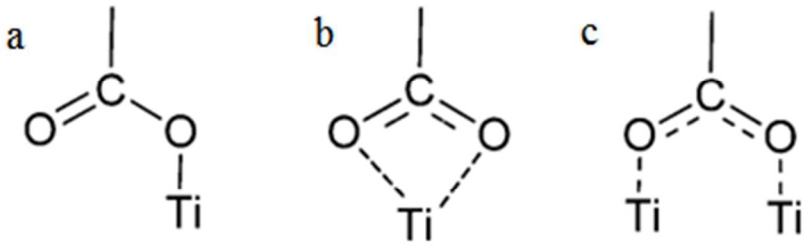


Chart 1: unidentate(a) bidentate chelating (b) and bidentate bridging(c) mode of carboxilate on $TiO_2$ surface

Similar to the carboxylate anchoring group, catechol can also bind to the $TiO_2$ surface in monodendate or bidentate modes. Li et al. [19] have shown that catechol can form two full-

coverage H-bonded structures, containing monodentate only or mixed monodentate- bidentate molecules on the $TiO_2$ surface (Chart 2). Monodentate and bidentate structures can simply convert into each other via proton exchange between catechol and the $TiO_2$ surface. In the bidentate mode, the formations of both bidentate mononuclear chelating (Chart 2b) and bidentate binuclear bridging (Chart 2c) complexes have been reported [27-29].

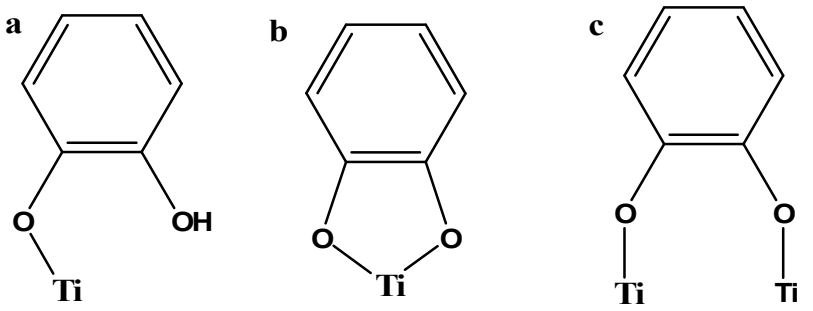


Chart 2: unidentate(a) bidentate chelating (b) and bidentate bridging(c) mode of catechol on $TiO_2$ surface

In this study, we used tetrakis(dihydroxyphenyl) Zinc(II) porphyrin (Zn-TDHPP) as sensitizer in dye sensitized solar cells and compared the results with tetrakis(p-carboxyphenyl) Zinc(II) porphyrin(ZnTCPP) which has been previously studied [22, 30]. To the best of our knowledge, this is the first report of a porphyrin dye with a catechol moiety anchoring group so far. Photosensitizers are characterized using NMR, FT-IR and UV-Vis spectroscopy. To investigate application of these sensitizers in DSSCs, the solution and solid state UV-Vis spectroscopy are used, and dye loading amount derived from these experiments. The current-voltage characteristics are also provided for the DSSCs with the synthesized photosensitizers. To obtain further evidences, density functional theory (DFT) calculations were carried out. Dye adsorption modeling was also used to investigate the adsorption kinetics and estimate electron injection

efficiencies from dye to $TiO_2$ surface. General structures of metaloporphyrins used in this study are shown in scheme 1.

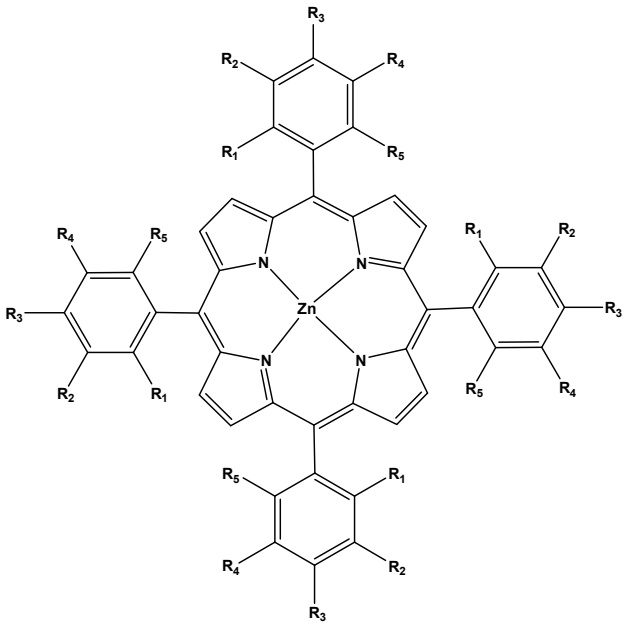


**Zn2,3TDHPP: R1,R2=OH R3,R4,R5=H**
**Zn3,4TDHPP: R2,R3=OH R1R4,R5=H**
**Zn2,4TDHPP: R1,R3=OH R2,R4,R5=H**
**Zn2,5TDHPP: R1,R4=OH R2,R3,R5=H**
**ZnTCPP: R3=COOH R1,R2,R4,R5=H**

Scheme1: General structures of sensitizers used in this study

## 2 Experimental

### 2.1 Materials and reagents

Tetrakis dihydroxyphenylporphyrins were obtained from Tetrakis dimethoxyphenylporphyrins (ZnTDMPP). The Tetrakis (dimethoxyphenyl)porphyrins and Tetrakis (p-carboxyphenyl)porphyrin were prepared by the condensation of the appropriate dimethoxybenzaldehyde with pyrrole in refluxing propionic acid [27]. The Tetrakis

dihydroxyphenylporphyrins were prepared by boron tribromide demethylation of the corresponding methyl ethers, according to the method presented by Milgrom [31]. Solvents were dried over appropriate drying agents. All other chemicals were reagent grade and used without further purification.

## 2.2 Analytical instruments and measurements

Solution absorption spectra were recorded on an Analytilc Jena s600 spectrometer using a 1 cm cuvette. Solutions were made at concentrations $5\times10^{-5}$M in ethanol. Solid state absorption spectra were recorded on a Shimadzo uv-2100 spectrometer.

$^{1}$H NMR and $^{13}$C NMR spectra were recorded in $DMSOd_6$ using a 300 MHz Bruker instrument. Photocurrent-voltage (I-V) measurements were performed using a Sharif solar (I-V) source measure unit and Prova 8300 sun simulator.

## 2.3 Synthesis of dyes

### 2.3.1 Tetrakis dimethoxyphenylporphyrins

Propionic acid (150 ml) was brought to a boil and then, the appropriate dimethoxybenzaldehyde (20 mmol) was added, followed by pyrrole (20 mmol) being added dropwise. After refluxing for 1.5h, the solution was cooled to room temperature and then crystallized over 3 days. The product was filtrated and washed with hot water and methanol. In the case of Tetrakis(3,4-Dimethoxyphenyl) Porphyrin and Tetrakis(2,5-Dimethoxyphenyl) Porphyrin no precipitate was achieved so the propionic acid was removed from crude. The solid black residue was purified using column chromatography with dichloromethane and methanol (50:1) as eluents.

Tetrakis(3,4-Dimethoxyphenyl) Porphyrin: Yield: 350 mg 4%, $^{1}$H NMR (CDCl3, 300 MHz), δ, ppm: 8.9 (s, 8H) , 7.8 (s, 4H), 7.7 (d, 4H) , 7.2 (d, 4H), 4.1 (s, 12H); 3.9 (s, 12H), -2.70 (s, 2H).

$^{13}$C NMR (CDCl3, 100 MHz), δ, ppm: 148.8, 147.0, 134.7, 131.1, 130.0, 127.34, 126.7, 119.8, 118.2, 110.2, 109.4, 108.7, 56.0, 55.9; UV– vis, (CHCl3 λmax): 421 (sorret); 518.; 556; 592; 649.

Tetrakis(2,3-Dimethoxyphenyl) Porphyrin: Yield: 680mg 8%, $^{1}$H NMR (300 MHz, CDCl3, 25℃): δ, ppm, 8.7(s, 8H), 7.2(m, 4H), 7.1(d, 4H), 7.0(m, 4H), 3.9 (s, 12H), 1.8 (s, 12H) -2.8(s, 2H).

Tetrakis(2,4-Dimethoxyphenyl) Porphyrin: Yield: 682mg 8%, $^{1}$H NMR (CDCl3, 300 MHz), δ, ppm, 8.7(s, 8H), 7.7(s, 4H), 7.0(s, 8H), 4.1 (s, 12H), 1.8 (s, 12H) , -2.7(s, 2H).

Tetrakis(2,5-Dimethoxyphenyl) Porphyrin: Yield: 500mg 6%,$^{1}$H NMR (CDCl3, 300 MHz), δ, ppm, 9 (s, 8H), 7.4 (d, 4H), 7.1 (s, 8H) -2.8(s, 2H), 3.9 (s, 12H), 1.9 (s, 12H) .

### 2.3.2 Tetrakis (p-carboxyphenyl)porphyrin (TCPP)

Propionic acid (150 mL) was brought to a boil and then the p-phthalaldehydic acid (20 mmol) was added followed by pyrrole (20 mmol) being added dropwise. After refluxing for 1.5 h, the solution was cooled to room temperature and then crystallized overnight. The product was filtrated and washed with hot water and a small amount of methanol.

Yield: 10%, $^{1}$H NMR (300 MHz, DMSO $d_6$, 25°C) δ (ppm): 8.7 (s, 8H), 8.3 (d, 8H), 8.1 (d, 8H), -2.9(s, 2H).

### 2.3.3 Zinc tetrakis (p-carboxyphenyl)porphyrin

A mixture of TCPP and 1.2eq $Zn(OAc)_2$.4H2O in methanol were stirred at room temperature. The metalation process was followed by Uv-vis spectroscopy. After the completion of the reaction, the solvent was evaporated with rotaevaporator at low temperature. The crude product

was washed several times with water to remove the excess zinc salt and then dried at low pressure using a vacuum pump.

Zn TCPP: Yield: 94%, $^{1}$H NMR (300 MHz, DMSO $d_6$, 25°C) δ (ppm): 8.9 (s, 8H), 8.4 (d, 8H), 8.3 (d, 8H). UV-vis (EtOH ,λmax, nm ):425 (soret), 558 , 601.

Tetrakis (dihydroxyphenyl)porphyrins(TDHPP)

The appropriate tetrakis (dimethoxyphenyl) porphyrin (0.5 mmol) was dissolved in the minimum amount of dry dichloromethane. The solution was cooled in a methanol-liquid nitrogen bath (to -98 °C). Boron tribromide (6 mmol) was slowly added to this solution. The mixture was stirred for 1 h at -98 °C, and then allowed to come to room temperature, and was then stirred overnight at room temperature. Water (20 mL) was added to quench the ice-cold reaction mixture. Neutralization with triethylamine produced a brown-purple precipitate, which was collected by filtration and washed with water and dichloromethane. Characterization for 3,4TDHPP: Yield: 75%, $^{1}$H NMR (300 MHz, DMSO$d_6$, 25°C): δ, ppm 9.4 (s, 8H), 8.9 (s, 8H), 7.7 (s, 4H), 7.4 (s, 4H), 7.1 (s, 4H), -2.9 (s, 2H). $^{13}$C NMR (75 MHz, DMSO$d_6$, 25 ° C): δ, ppm 145.0, 144.1, 132.8, 131.6, 126.7, 122.9, 120.4, 115.9, 114.7. IR (KBr): ν, cm-1 3386, 1653, 1597, 1508, 1433, 1346, 1260, 1201, 1108, 928, 871, 801, 711. UV-vis (EtOH ,λmax, nm ): 428 (soret), 520 , 559 , 592 , 653.

2,3TDHPP: Yield: 80%, $^{1}$H NMR (300 MHz, DMSO-$d_6$, 25℃): δ, ppm 9.7 (s, 8H), 8.7(s, 8H), 7.2(m, 4H), 7.1(d, 4H), 7.0(m, 4H), -2.8(s, 2H). $^{13}$C NMR (75MHz, DMSO-d6, 25℃): δ, ppm, 146.5, 145.5, 129.1, 128.6, 127.8, 126.8, 118.1, 116.8, 116.1. IR (KBr): ν, cm-1, 3423, 2923, 2853, 1615, 1586, 1466, 1346, 1204, 1145, 927, 844, 804, 768, 730. UV-Vis (EtOH, λmax, nm): 420 (soret), 516,550, 591, 647.

2,4TDHPP: Yield: 78%, $^{1}$H NMR (300 MHz, DMSO-$d_6$, 25℃): δ, ppm 9.1 (s, 8H), 8.8(s, 8H), 7.7(s, 4H), 7.0(s, 8H), -2.7(s, 2H). $^{13}$C NMR (75MHz, DMSO-d6, 25℃): δ, ppm, 146.5, 145.5, 129.1, 128.6, 127.8, 126.8, 118.1, 116.8, 116.1

### 2.3.4 Zn- Tetrakis (dihydroxyphenyl)porphyrins

A mixture of TDHPP and 1.2eq $Zn(OAc)_2.4H_2O$ in methanol were stirred at room temperature. The metalation process was followed by uv-vis spectroscopy. After the completion of the reaction, the solvent was evaporated with a rotaevaporator at low temperature. The crude product was washed several times with water to remove the excess zinc salt and then dried at low pressure using a vacuum pump.

Zn2,3TDHPP: Yield:95%, $^{1}$H NMR (300 MHz, DMSO-$d_6$, 25℃): δ, ppm 9.7 (s, 8H), 8.8(s, 8H), 7.4(m, 4H), 7.2(d, 4H), 7.0(m, 4H).$^{13}$C NMR (75MHz, DMSO-d6, 25℃): δ, ppm, 146.6, 145.5, 129.2, 128.8, 128.0, 126.8, 118.3, 116.9, 115.9. IR (KBr): ν, cm-1, 3426, 2926, 2851, 1620, 1586, 1466, 1346, 1210, 1145, 927, 844, 809, 768, 735,547 ,469. UV-vis (EtOH ,λmax, nm ): 425 (soret), 556 , 592. Elemental Analysis Calc. for C44H28N4O8Zn: C, 65.56; H, 3.50; N, 6.95; Found C, 65.58; H, 3.45; N, 6.98%.

Zn 3,4TDHPP: Yield:95%, $^{1}$H NMR (300 MHz, DMSO$d_6$, 25°C): δ, ppm 9.4 (s, 8H), 8.8 (s, 8H), 7.7 (s, 4H), 7.4 (s, 4H), 7.1 (s, 4H), $^{13}$C NMR (75 MHz, DMSO$d_6$, 25 ° C): δ, ppm 145.0, 144.1, 132.8, 131.6, 126.7, 122.9, 120.4, 115.9, 114.7. UV-vis (EtOH ,λmax, nm ): 428 (soret), 559 , 602.

Zn 2,4TDHPP: Yield:96%, $^{1}$H NMR (300 MHz, DMSO$d_6$, 25°C): δ, ppm 9.4 (s, 8H), 8.8 (s, 8H), 7.7 (s, 4H), 6.9 (s, 8H). UV-vis (EtOH ,λmax, nm ): 425 (soret), 556 , 597.

Zn 2,5TDHPP: Yield:95%, $^{1}$H NMR (300 MHz, DMSO$d_6$, 25°C): δ, ppm 9.7 (s, 8H), 9 (s, 8H), 7.4 (d, 4H), 7.1 (s, 8H). UV-vis (EtOH ,λmax, nm ): 424 (soret), 556 , 591.

## 2.4 Fabrication of dye-sensitized solar cells and photovoltaic measurements

### 2.4.1 Preparation of nanoporous $TiO_2$ paste

Two kinds of $TiO_2$ paste containing nanocrystalline $TiO_2$ (20 nm, paste A) and submicroparticle $TiO_2$ (350 nm, paste B) were prepared by a previously reported procedure [32, 33]. 3 g of $TiO_2$ nanopowder was added to mortar and grinded with gradual addition of 0.5 ml of acetic acid, 2.5 ml of deionized water and 15 ml of ethanol. The $TiO_2$ dispersion was transferred with 50 ml of ethanol to a round bottom flask and homogenized by an ultrasonic bath for 30 min. 10 g of terpineol was added to the dispersion and sonication was resumed for another 30 min. Alternating stirring and sonication were used three consecutive times after adding 1.5 g of ethyl cellulose (10% solution in ethanol) to the $TiO_2$ dispersion. Finally ethanol was removed by a rotary evaporator. The resulting screen-printing paste corresponds to 21 wt.% $TiO_2$, 10 wt.% ethyl cellulose and 69 wt.% terpineol (paste A).

Paste B which was used in the light-scattering layers was prepared with the same method using 350 nm $TiO_2$ nanoparticles.

### 2.4.2 Fabrication of porous-$TiO_2$ electrodes

The FTO glass was first cleaned with detergent solution, distilled water and methanol using an ultrasonic bath (10 min for each solution), and then rinsed with methanol. After treatment in 40 mM aqueous $TiCl_4$ solution at 70 °C for 30min, the FTO glass was again washed with water and methanol. Paste A was screen printed (manual screen printer, 90T, Estal Mono, Schweiz. Seidengazefabrik, AG, Thal) on the FTO glass and kept in a clean box for 10 min to let the paste

relax and reduce the surface irregularity. After that, FTO glasses were dried for 10 min at 125 °C. This screen printing procedure with paste A (coating, storing and drying) was repeated to get an appropriate thickness of 10–12 μm for the working electrode. After drying the (paste A) films at 125 °C, one layer of paste B was deposited by the screen-printing method, resulting in a light-scattering $TiO_2$ film containing 350 nm anatase $TiO_2$ particles. The electrodes coated with the $TiO_2$ pastes were gradually heated under airflow at 325 °C for 5 min, at 375 °C for 5 min, and at 450 °C for 15min, and finally, at 500 °C for 15 min.

The $TiO_2$ films were once again treated with 40 mM $TiCl_4$ solution, as previously described, then rinsed with water and methanol and heated at 450 °C for 15 min and 500 °C for 15 min. After cooling to 80 °C, the $TiO_2$ electrodes were immersed into 0.1 mM dye solution with 35 mM 4-tert-Butylpyridine as additive in a mixture of ethanol and THF (volume ratio, 4:1) and kept at room temperature for 2 h to uptake the dye.

### 2.4.3 Preparation of counter Pt-electrodes and DSSC assemblage

FTO glasses were washed with the same method as used for the working electrode. 0.05 M $H_2PtCl_6$ solution was spin-coated on the FTO glass substrate at 2000 rpm for 15 s. The formed film was annealed at 450 °C for 1 hour in atmosphere.

Clamps assembled the dye-adsorbed $TiO_2$ electrode and counter electrode into a sandwich-type cell. Finally a drop of electrolyte solution (0.10 M lithium iodide, 0.60 M butylmethylimidazolium iodide, 0.03 M I2, and 0.05 M 4-tert-butylpyridine in acetonitrile/valeronitrile 75:25) was introduced into the clamped electrodes.

## 2.5 Desorption measurement

The amounts of dye-loading of each dye determined by dye desorption in a basic solution. The dye loaded anodes were soaked in 10%

solution of tetrabuthylammonium hydroxide in water/EtOH. The solutions absorbances were measured during the time till the dyes completely desorbed from electrode.

# 3 RESULTS AND DISCUSSION

We have studied four types of porphyrin dyes, Zn2,3TDHPP, Zn2,4TDHPP, Zn2,5TDHPP, Zn3,4TDHPP and compared them with previously studied dye ZnTCPP (scheme1). Each of these dyes was chosen because they have two hydroxyl groups on each porphyrin meso phenyls as anchoring groups. In the case of Zn-2,3TDHPP and Zn-3,4TDHPP these two hydroxyl groups were adjacent and cooperatively bond to $TiO_2$ surface but for Zn-2,4TDHPP and Zn-2,5TDHPP they were non-adjacent.

## 3.1 Photophysical properties of the dyes in solution and on $TiO_2$ film

### 3.1.1 Photophysical properties of the dyes in solution

Uv-vis spectra of metaloporphyrins are shown in figure 1. Absorption spectra were measured between 400 and 750 nm in ethanolic solutions. All studied metalloporphyrins have strong soret bands at around 425 – 428 nm and two Q bands at around 500 - 700 nm which are uv-vis spectra characteristics of metalloporphyrins and makes them potential candidates for light harvesting in DSSCs.

Zinc is a closed shell metal and has very little effect on the porphyrin $\pi$ to $\pi^*$ energy gap in porphyrin electronic spectra. The soret band for Zn-TDHPPs was 5 -8 nm red shifted relative to zinc tetraphenylporphyrin which indicates the conjugation of the lone-pair electrons of the eight

oxygen atoms that are directly attached to the phenyl rings, with π electrons of the macrocycle rings [18, 34]. Extinction coefficients for Zn-TDHPPs were lower than ZnTPP due to both electronic and steric effects [35, 36]. Zn-TDHPPs with adjacent hydroxyl groups have relatively higher extinction coefficients than the porphyrins with non-adjacent hydroxyl groups. The lower extinction coefficient in such porphyrins i.e. Zn2,5TDHPP, could be due to the resonance forms shown in chart3 [37]. The π system extension, results in a red shift in the porphyrin uv-vis spectra and the electronegativity of oxygen, attracts electron density from the porphyrin ring and lowered the extinction coefficient [36].

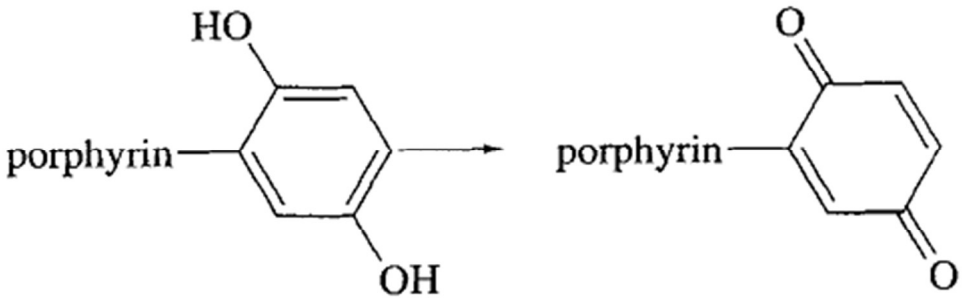


Chart3. The resonance forms of 2,5TDHPP

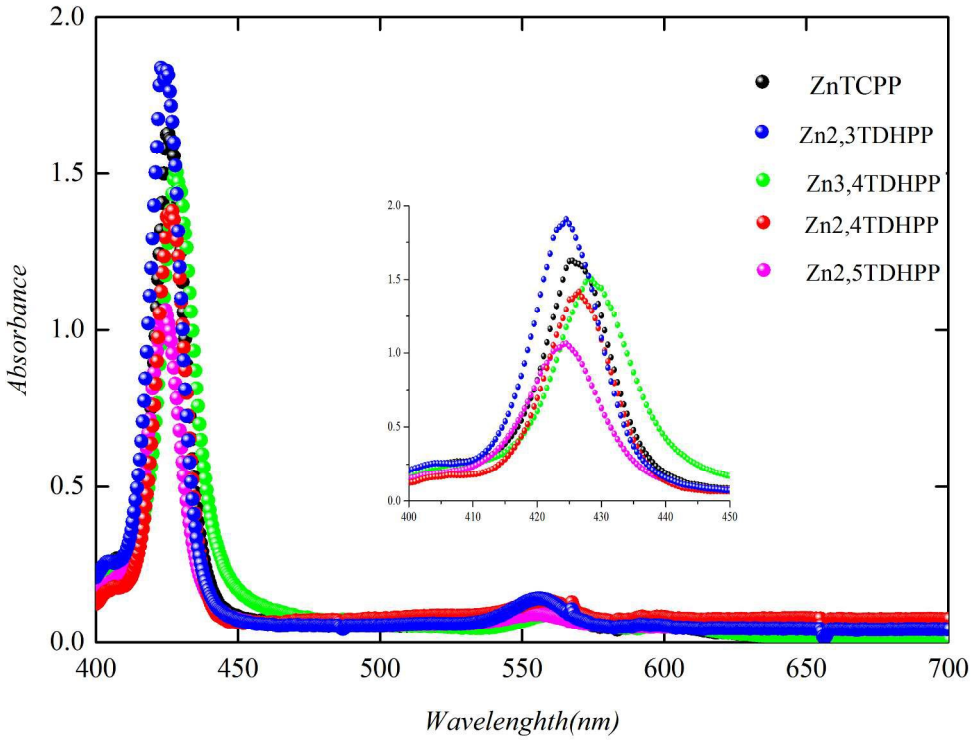


Figure1. Uv-vis spectra of metalloporphyrins at 0.05mM concentration

### 3.1.2 Photophysical properties of the dyes adsorbed on the $TiO_2$ film

The solid state uv-vis spectra of zinc tetrakis(dihydroxyphenyl) porphyrin and zinc tetrakis(p-carboxyphenyl) porphyrin dyes adsorbed on the $TiO_2$ film have been shown in fig 2. The broadened absorption bands of the dyes on $TiO_2$ might be a sign of intermolecular interactions of the molecules aggregated on the $TiO_2$ surfaces [38]. All zinc tetrakis(dihydroxyphenyl) porphyrin dyes have sharper soret band to that of ZnTCPP indicating lower aggregation in former compounds. Dihydroxophenylporphyrins also show red shift upon binding to the $TiO_2$ film which could be ascribed to the stabilization of the LUMO level in $TiO_2$-Porphyrin complexes[39]. In the case of ZnTCPP the existence of blue shoulders for the soret bands may have been derived

from the deprotonation of the carboxylic acid upon binding to the $TiO_2$ surface [40] and/or H-type aggregation of the dye molecules[41, 42].

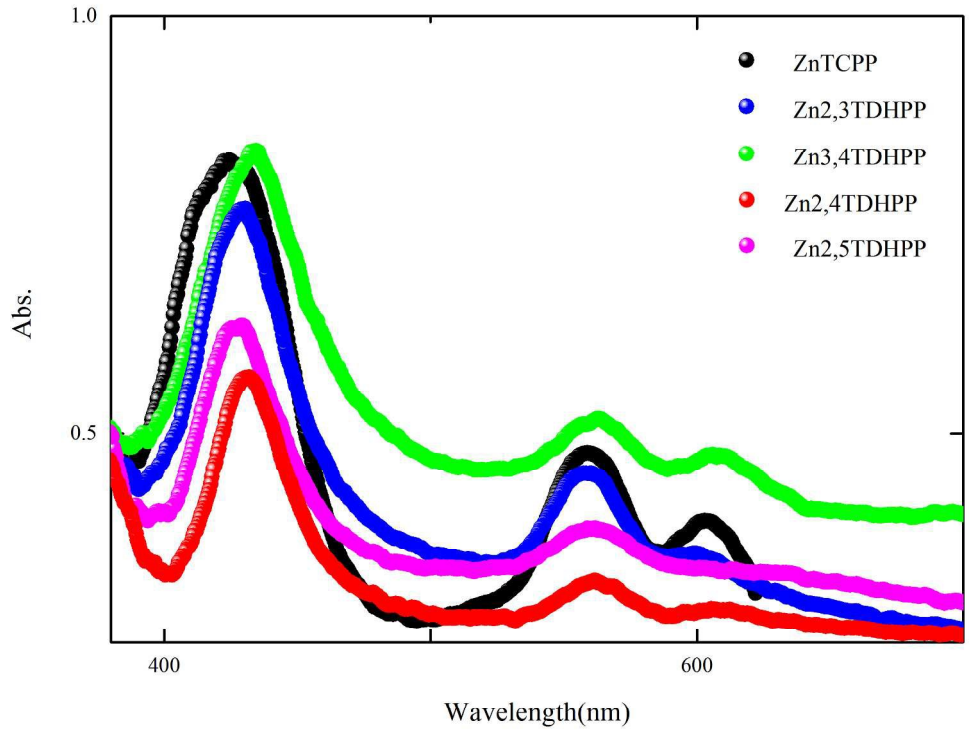


Figure 2. The solid state uv-vis spectra of ZnTDHPP dyes adsorbed on the $TiO_2$ film

### 3.1.3 Desorption of dyes from $TiO_2$ film and adsorption model

In order to measure dye loading amount and also the time for complete desorption of dye from $TiO_2$ surface we carried an experiment to desorb of dye from $TiO_2$ surface. Figure 3 shows desorption of dyes from the $TiO_2$ surface versus time in TBAOH solution.

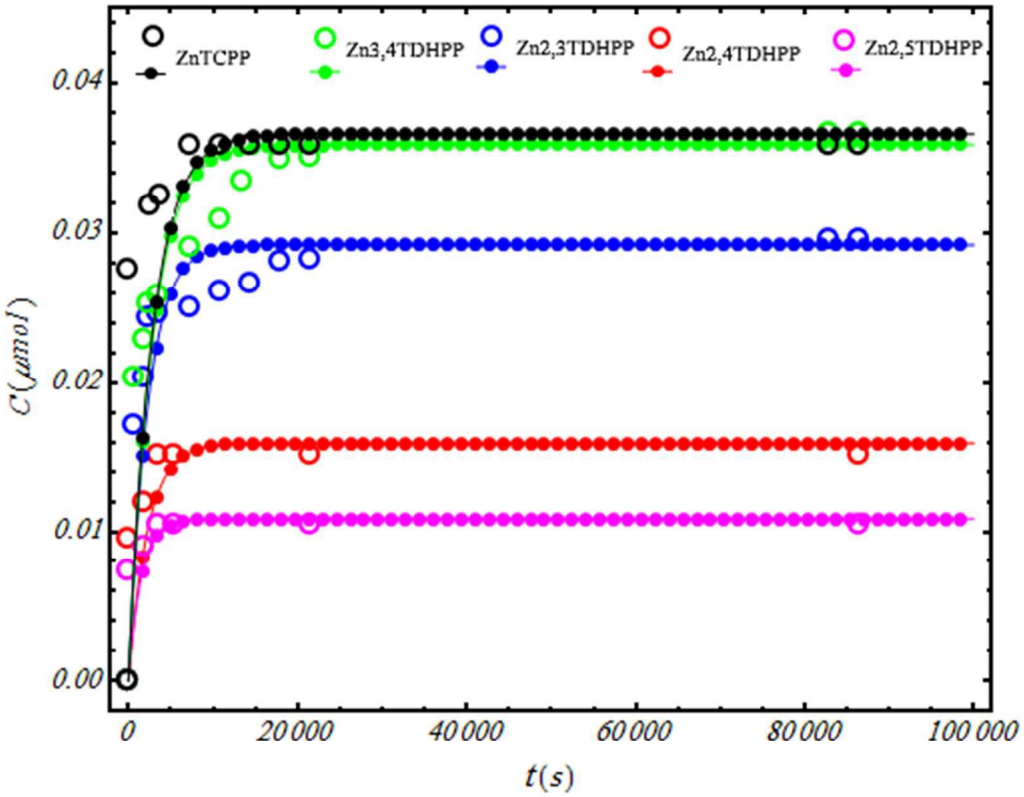


Figure 3. Desorption of dyes from $TiO_2$ surface during the 30 hrs (O-experimental ●-model).

ZnTCPP and porphyrins with non-adjacent hydroxyl groups desorbed from $TiO_2$ surface very quickly; in comparison Zn2,3TDHPP and Zn3,4TDHPP desorbed more slowly from the $TiO_2$ surface. Zn2,4TDHPP and Zn2,5TDHPP almost completely desorbed from the $TiO_2$ surface after 30 minute and ZnTCPP after two hours yet this process took six hours for Zn2,3TDHPP and Zn3,4TDHPP. There was no significant desorption in acidic and neutral media after days. Therefore Zn2,3TDHPP and Zn3,4TDHPP showed almost three times more stability on $TiO_2$ surface. This significant increase in stability of catechol anchoring group can arise from cooperative bonding of dihydroxy phenyl via stable five member ring (form b in chart2).

Table 1 shows data concerning spectral properties and dye loading amount of all the synthesized porphyrin derivatives on the $TiO_2$ surface calculated from desorption and calibration data.

For non-adjacent hydroxyl group dyes, the loading amount and also desorption time were very low, which indicates that in such porphyrins, there was no effective attachment of dye on the $TiO_2$ surface. Although all of the electrodes were soaked in dye solutions of the same concentration for the same period of time, the amount of adsorbed dye forZn2,3TDHPP was lower than Zn3,4TDHPP. This observation suggests that the flat orientation of adsorbed porphyrin with respect to the $TiO_2$ surface of Zn2,3TDHPP(25.3 nmol.cm$^{-2}$) results in less dye intake compared to Zn3,4TDHPP (36.7 nmol.cm$^{-2}$) and ZnTCPP ( 33.5 nmol.cm$^{-2}$) [20, 43] (Figure4).

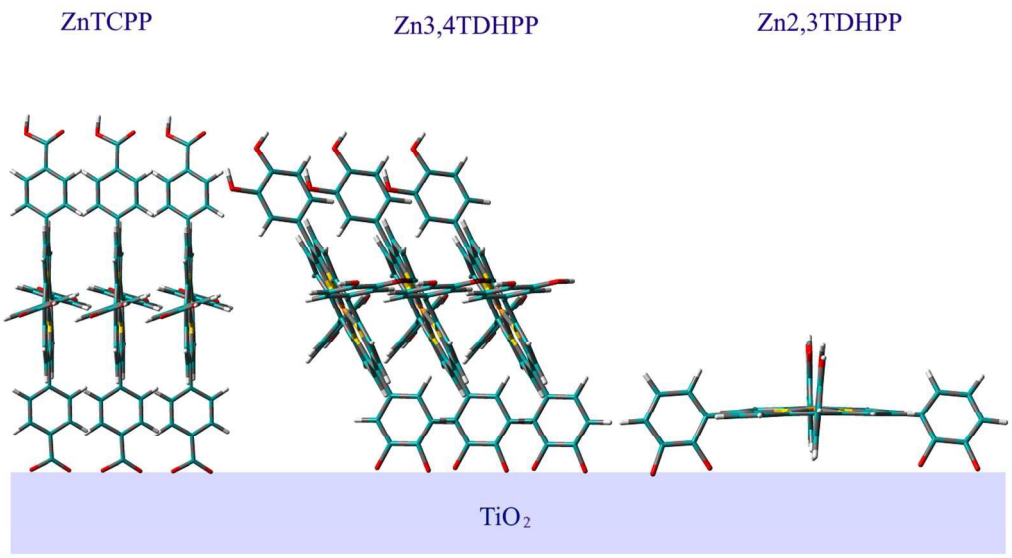


Figure 4 . Orientation of adsorbed porphyrin with respect to the $TiO_2$ surface

Here, we implement a model, developed in our previous work [44], for investigation of time evolution of dye loading to extract the dye adsorption. The adsorption from dye solution by solid nanoparticle is studied assuming kinetic form of the time dependent Langmuir formalism

framework. In the present microscopic model it is assumed that the bulk density of dye molecules are adsorbed only by nanoparticles network by a constant adsorption and desorption rates, also the interconnection of nanoparticles is influenced by particle necking which leads to partial aggregation of nanoparticles.

Using $k_a$ and $k_d$ as the rate constants for adsorption and desorption, respectively, we can write the net rate of adsorption for solution phase species i as the difference between the rate of adsorption and the rate of desorption:

$$R_{i,ads,net} = k_{ai}C_{isol}\left(C_{i-site,total} - C_{i-sites,occupied\ by\ i}\right) - k_{d,s}C_{i-sites,occupied\ by\ i} \quad (1)$$

which means that the rate of adsorption should be proportional to the concentration of dye molecules in the solution phase ($C_{isol}$) and to the number of sites available on the surface of particles. If the dye molecules in the solution around the adsorbent solid particles occupy some fraction $\in$ of a volume V, and if this volume contains an adsorbing dye molecule i, then the rate of adsorption of the dye molecules onto the adsorbent and the rate of depletion of that species from the solution phase are coupled batch processes. The component mass balances for the solution and solid phases are as follows

Solution phase

$$\frac{dC_{i,sol}\in V}{dt} = -(1-\in)R_{i,ads,net}A_s\rho_s V \quad (2)$$

Solid phase

$$\frac{dC_{i,s}(1-\in)A_{tot}}{dt} = (1-\in)R_{i,ads,net}A_s\rho_s V \quad (3)$$

where $A_s$ is effective surface area of nanoparticle matrix per unit of mass and $\rho_s$, solid nanoparticle density. The further derivation of equations can be found in literature[44]. The obtained adsorption amount on the semiconductor matrix can be assumed to calculate the injection efficiency by relation 4.

$$\varphi_{inj} = \varphi(1 - 10^{-C_a}) \quad (4)$$

The highest rate of injection efficiency belongs to ZnTCPP. The estimated injection quantum yield together with 100% collection efficiency in DSSCs,44 strongly suggest that the limiting performance factor for DSSCs can be the inefficient injection efficiency of the cells (Table1).

Table 1. Absorption wavelength, extinction coefficient and loading amount of dyes on $TiO_2$

| dye | $\lambda_{max}$ (nm) ethanol | $\varepsilon\times10^{-5}$ ($M^{-1}cm^{-1}$) | $\lambda_{max}$ (nm) on $TiO_2$ surface | Dye loading ($nmol.cm^{-2}$) | Injection efficiency %($\varphi_{inj}$) | Adsorption coefficient($k_a$) $nmol/cm^{-1}$ | Desorption coefficient-($k_d$) $nmol/cm^{-1}$ |
|---|---|---|---|---|---|---|---|
| ZnTCPP | 425 | 3.466 | 425 | 33.5 | 2.63 | $100*10^{-3.0}$ | $2.85*10^{-3.9}$ |
| Zn2,3TDHPP | 425 | 4.538 | 430 | 25.3 | 2.6 | $100*10^{-3.1}$ | $3.5*10^{-3.9}$ |
| Zn3,4TDHPP | 428 | 3.098 | 435 | 36.7 | 2.5 | $100*10^{-3.01}$ | $2.85*10^{-3.9}$ |
| Zn2,5TDHPP | 424 | 2.84 | 429 | 15.1 | 0.9 | $57*10^{-3.01}$ | $3.8*10^{-3.75}$ |
| Zn2,4TDHPP | 425 | 2.24 | 432 | 10.4 | 0.5 | $55*10^{-3.01}$ | $2.5*10^{-3.75}$ |

## 3.2 Photovoltaic properties

To consider the potential of Zn-TDHPP as photosensitizers for DSSC, their DSSCs performances were tested. Fig 5 shows J-V curves for the studied dyes. Detailed photovoltaic parameters such as open circuit voltage ($V_{OC}$), short circuit current ($J_{SC}$), filling factor (FF) and power conversion efficiency (η) for different dyes under AM 1.5 solar illumination have been listed in Table 2. power conversion efficiency is derived from the equation: $\eta = J_{SC} \times V_{OC} \times ff$, where $J_{SC}$ is the short circuit current, $V_{OC}$ is the open circuit potential, and ff is the fill factor.

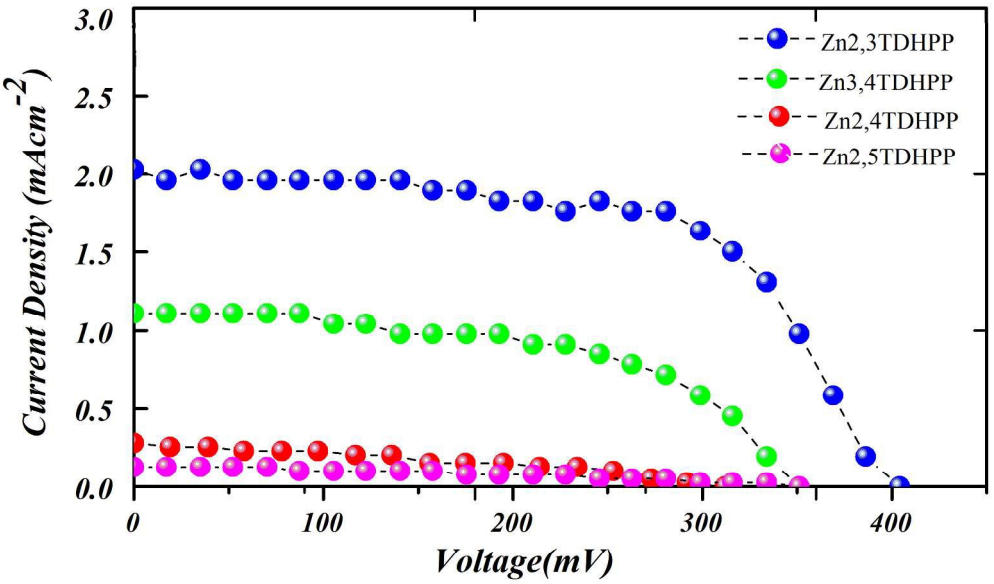


Figure 5. Current-voltage curves for DSSCs based on Zn2,3TDHPP, Zn3,4TDHPP, Zn2,4TDHPP and Zn2,5TDHPP under illumination of AM 1.5 simulated sunlight

The $V_{OC}$ values of all the dye cells ranked: ZnTCPP = Zn2,3TDHPP > Zn3,4TDHPP > Zn2,5TDHPP > Zn2,4TDHPP. Despite the lower dye loading amount for Zn2,3TDHPP compared to ZnTCPP and Zn3,4TDHPP; the Voc value for this porphyrin is similar to ZnTCPP. This could be because of the flat orientation of Zn2,3TDHPP on the $TiO_2$ surface, meaning it could cover the surface more than the other dyes and prevent direct contact of electrolyte with $TiO_2$ as well as decrease the recombination.

Similar to power conversion efficiencies, the Jsc values of all the dye cells ranked: ZnTCPP > Zn2,3TDHPP > Zn3,4TDHPP > Zn2,4TDHPP > Zn2,5TDHPP. The order is the same as extinction coefficient for ZnTDHPPs indicating that short circuit current increases with increase

in light absorption ability. However, in the case of Zn-2,4-TDHPP and Zn-2,5-TDHPP photovoltaic results were poor because of weak binding on $TiO_2$ surface and in some extent due to lower extinction coefficients of the corresponding dye**.**

Table 2. Photovoltaic parameters of porphyrin-based dye-sensitized solar cells under AM 1.5 illumination

| Dye | Voc(mV) | Jsc ($mAcm^{-2}$) | Fill factor(%) | Efficiency(%) |
|---|---|---|---|---|
| ZnTCPP | 449 | 2.7 | 67 | 0.8 |
| Zn2,3TDHPP | 449 | 2.1 | 62 | 0.6 |
| Zn3,4TDHPP | 410 | 1.11 | 51 | 0.23 |
| Zn2,4TDHPP | 312 | 0.28 | 34 | 0.03 |
| Zn2,5TDHPP | 390 | 0.12 | 38 | 0.02 |

### 3.3 Density functional theory (DFT) calculations:

To obtain further evidences for the above results, DFT calculations of two porphyrins with adjacent hydroxyl group and ZnTCPP dyes were carried out, using the B3LYP/3-21G level. The calculated structures do not show negative frequencies, inferring that the optimized geometries are in the global energy minima. Figure 6 illustrates the electron density distributions of dyes in their respective HOMO and LUMO levels. The energy levels of frontier orbitals and the HOMO - LUMO energy gaps for these three dyes are listed in table3.

Electron distributions of all three dyes, in the frontier orbitals, are mostly over the porphyrin ring which is likely due to the fact that the phenyl rings are perpendicular to the porphyrin ring and do not contribute to electron distributions. This could block electron transfer to $TiO_2$ and reduce photovoltaic performance for studied dyes to those that have anchoring group participate in electron conjugation. It is well known that the electron density distribution of LUMO around an

anchoring group , affect the electronic coupling between the excited adsorbed dye and 3d orbital of $TiO_2$[45]. Consequently, we can expect the low φinj values of dyes (table1).

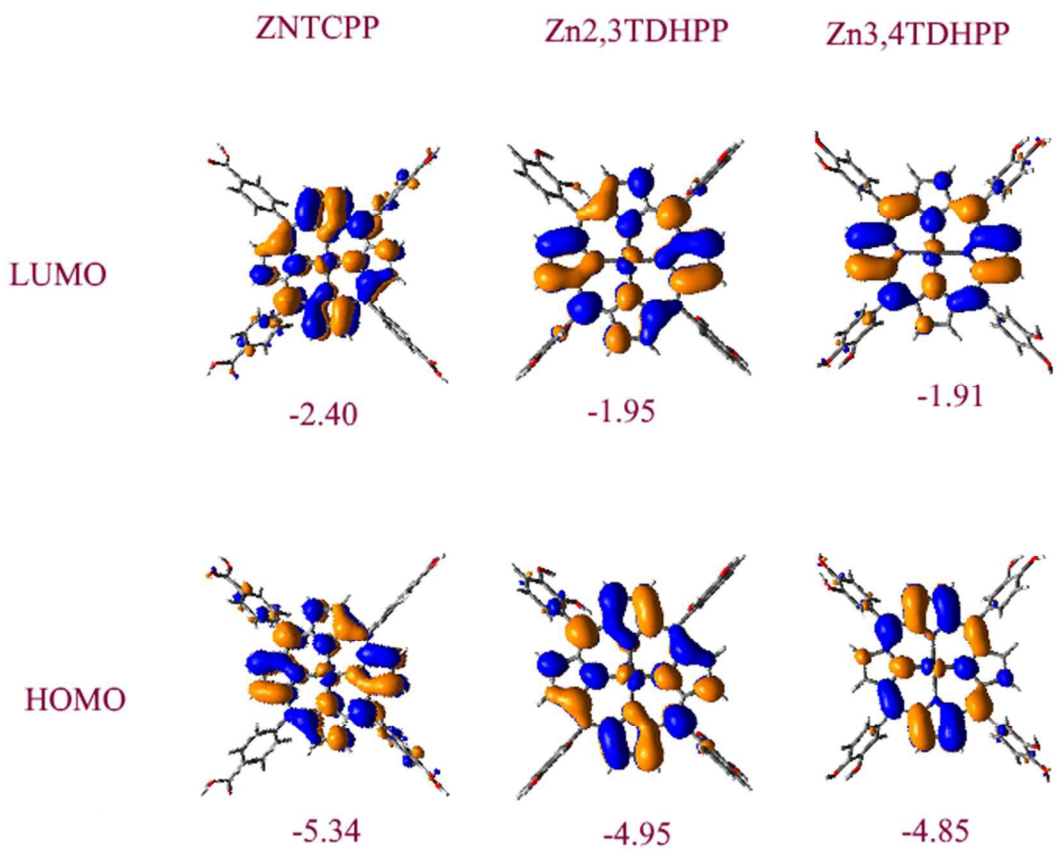


Figure 6. The electron density distributions and energy levels of ZnTCPP, Zn2,3TDHPP and Zn3,4TDHPP

For ZnTDHPPs, variations in energies for different positions of the hydroxyl groups for the HOMO level (-4.95eV for Zn2,3TDHPP and -4.85 eV for Zn3,4TDHPP) are larger than those for the LUMO level (-1.91 eV for Zn2,3TDHPP and -1.95 eV for Zn3,4TDHPP); indicating that variations in the hydroxyl group position mainly affect the occupied orbitals of ZnTDHPP dyes (table3). In addition, dihedral angle between phenyl unit and the porphyrin macrocycle for Zn2,3TDHPP is 84.1° but the corresponding angle for

Zn3,4TDHPP and ZnTCPP is 69.1° and 69.5°; indicating that Zn2,3TDHPP is more nonplanar than the others.

It is well known that for nonplanar and distorted dyes, dye aggregation and charge recombination can be efficiently suppressed, which is favorable for enhancing cell efficiency[42]. Similarly lower Voc for Zn3,4TDHPP could be a consequence of the lower dihedral angle between the phenyl unit and the porphyrin macrocycle and the more planar structure which favors aggregation. Therefore, Zn2,3TDHPP, compared to Zn3,4TDHPP could be considered a better dye due to its different mode of attachment,Fig4, and its relatively nonplanar structure [8, 42, 46].

Table3. The energy levels of frontier orbitals and the HOMO - LUMO energy gaps for ZnTCPP,Zn2,3TDHPP and Zn3,4TDHPP

| Dye | HOMO(eV) | LUMO(eV) | $E_g$ |
|---|---|---|---|
| ZnTCPP | -5.34 | -2.40 | 2.94 |
| Zn2,3TDHPP | -4.95 | -1.91 | 3.03 |
| Zn3,4TDHPP | -4.85 | -1.95 | 2.9 |

In order to have fast electron transfer, the HOMO must be sufficiently more positive than the redox potential of $I^-/I_3^-$ to accept electrons effectively; the difference between these two levels is given by ΔE [47]. HOMO energy levels are -5.34,-4,95 and -4.85 for ZnTCPP, Zn2,3TDHPP and Zn3,4TDHPP respectively; considering that $I^-/I_3^-$ electrolyte potential is -4.85eV[48] the differences between electrolyte and HOMO energy level (ΔE) are 0.5, 0.1 and 0 for ZnTCPP, Zn2,3TDHPP and Zn3,4TDHPP. For Zn3,4TDHPP there is no driving force for electron

injection from electrolyte to dye oxidized state that could be the reason of poor photocurrent in this dye (figure 7) [47].

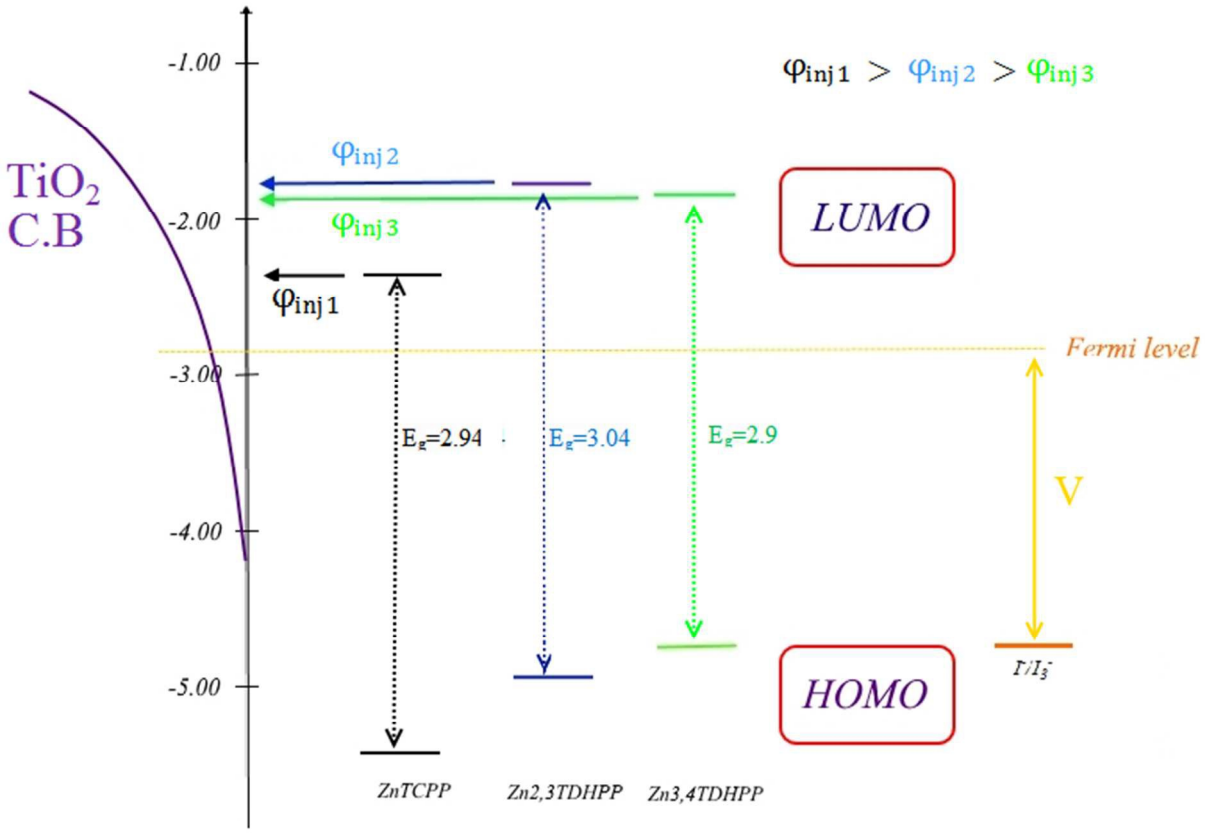


Figure 7. Illustration of energy levels and electron injection efficiencies of ZnTCPP, Zn2,3TDHPP and Zn3,4TDHPP

## 4 Conclusion

Zn-TDHPP dyes were successfully synthesized and used as sensitizer in DSSCs and compared with ZnTCPP as reference dye. This is the first report of a porphyrin dye with a catechol anchoring group so far. The Jsc values of all the dye cells as well as power conversion

efficiencies, were ranked: ZnTCPP > Zn2,3TDHPP > Zn3,4TDHPP > Zn2,4TDHPP > Zn2,5TDHPP; The order was the same as extinction coefficient for ZnTDHPPs. Despite lower dye loading on $TiO_2$ surface for Zn2,3TDHPP it has comparable photovoltaic performance(0.6 vs. 0.9) and more stability to ZnTCPP. The stability of the dye on $TiO_2$ for Zn2,3TDHPP and Zn3,4TDHPP might arise from bidandate coordination on $TiO_2$ surface via chelating and formation of five member ring. The higher efficiency observed for Zn2,3TDHPP relative to Zn3,4TDHPP may be ascribed to, mode of coordination to the $TiO_2$ surface which result in more efficient electron transfer, suppressed dye aggregation and high extinction coefficient for the former compound. Injection efficiencies of the cells were also calculated; the results indicate that the limiting performance factor for DSSCs can be the inefficient injection efficiency of the cells. Future strategy is to get advantage of high stability of catechole anchoring group and extend π system contibution and also synthesis of asymmetric porphyrins to make dipole moment by modification of porphyrin core to enhance the efficiencies.

## 5 Acknowledgments:

This work was supported by the Iranian National Science Foundation (INSF) and Shahid Beheshti University Research Affaires.

**References:**

1. B. O'Regan and M. Gratzel, *Nature*, 1991, **353**, 737-740.
2. A. Hagfeldt, G. Boschloo, L. Sun, L. Kloo and H. Pettersson, *Chemical Reviews*, 2010, **110**, 6595-6663.
3. M. K. Nazeeruddin, E. Baranoff and M. Grätzel, *Solar Energy*, 2011, **85**, 1172-1178.
4. M. Grätzel, *Journal of Photochemistry and Photobiology C: Photochemistry Reviews*, 2003, **4**, 145-153.

5. N. Xiang, X. Huang, X. Feng, Y. Liu, B. Zhao, L. Deng, P. Shen, J. Fei and S. Tan, *Dyes and Pigments*, 2011, **88**, 75-83.
6. A. Yella, H. W. Lee, H. N. Tsao, C. Yi, A. K. Chandiran, M. K. Nazeeruddin, E. W. G. Diau, C. Y. Yeh, S. M. Zakeeruddin and M. Grätzel, *Science*, 2011, **334**, 629-634.
7. S. Eu, S. Hayashi, T. Umeyama, Y. Matano, Y. Araki and H. Imahori, *The Journal of Physical Chemistry C*, 2008, **112**, 4396-4405.
8. H.-P. Wu, Z.-W. Ou, T.-Y. Pan, C.-M. Lan, W.-K. Huang, H.-W. Lee, N. M. Reddy, C.-T. Chen, W.-S. Chao, C.-Y. Yeh and E. W.-G. Diau, *Energy & Environmental Science*, 2012, **5**, 9843-9848.
9. D. Arteaga, R. Cotta, A. Ortiz, B. Insuasty, N. Martin and L. Echegoyen, *Dyes and Pigments*, 2015, **112**, 127-137.
10. T. Hasobe, S. Hattori, P. V. Kamat, Y. Urano, N. Umezawa, T. Nagano and S. Fukuzumi, *Chemical Physics*, 2005, **319**, 243-252.
11. A. Yella, C.-L. Mai, S. M. Zakeeruddin, S.-N. Chang, C.-H. Hsieh, C.-Y. Yeh and M. Grätzel, *Angewandte Chemie*, 2014, **126**, 3017-3021.
12. S. Mathew, A. Yella, P. Gao, R. Humphry-Baker, B. F. Curchod, N. Ashari-Astani, I. Tavernelli, U. Rothlisberger, M. K. Nazeeruddin and M. Grätzel, *Nature chemistry*, 2014.
13. D. Daphnomili, G. D. Sharma, S. Biswas, K. R. Justin Thomas and A. G. Coutsolelos, *Journal of Photochemistry and Photobiology A: Chemistry*, 2013, **253**, 88-96.
14. H. Deng, Z. Lu, Y. Shen, H. Mao and H. Xu, *Chemical physics*, 1998, **231**, 95-103.
15. R. Mosurkal, J.-A. He, K. Yang, L. A. Samuelson and J. Kumar, *Journal of Photochemistry and Photobiology A: Chemistry*, 2004, **168**, 191-196.
16. S. Osati, S. S. H. Davarani, N. Safari and M. H. Banitaba, *Electrochimica Acta*, 2011.
17. S. Osati, N. Safari, M. K. Bojdi and S. S. H. Davarani, *Journal of Electroanalytical Chemistry*, 2011.
18. S. Shahrokhian and A. Hamzehloei, *Electrochemistry Communications*, 2003, **5**, 706-710.
19. S.-C. Li, J.-g. Wang, P. Jacobson, X. Q. Gong, A. Selloni and U. Diebold, *Journal of the American Chemical Society*, 2009, **131**, 980-984.
20. W. M. Campbell, A. K. Burrell, D. L. Officer and K. W. Jolley, *Coordination Chemistry Reviews*, 2004, **248**, 1363-1379.
21. J. Rochford, D. Chu, A. Hagfeldt and E. Galoppini, *Journal of the American Chemical Society*, 2007, **129**, 4655-4665.
22. S. Cherian and C. C. Wamser, *The Journal of Physical Chemistry B*, 2000, **104**, 3624-3629.
23. A. Kay and M. Graetzel, *The Journal of Physical Chemistry*, 1993, **97**, 6272-6277.
24. K. Kalyanasundaram, N. Vlachopoulos, V. Krishnan, A. Monnier and M. Graetzel, *The Journal of Physical Chemistry*, 1987, **91**, 2342-2347.
25. H. Imahori, S. Hayashi, H. Hayashi, A. Oguro, S. Eu, T. Umeyama and Y. Matano, *The Journal of Physical Chemistry C*, 2009, **113**, 18406-18413.
26. M. K. Nazeeruddin, R. Humphry-Baker, P. Liska and M. Grätzel, *The Journal of Physical Chemistry B*, 2003, **107**, 8981-8987.
27. I. A. Janković, Z. V. Šaponjić, M. I. Čomor and J. M. Nedeljković, *The Journal of Physical Chemistry C*, 2009, **113**, 12645-12652.
28. P. Z. Araujo, P. J. Morando and M. A. Blesa, *Langmuir*, 2005, **21**, 3470-3474.
29. P. Z. Araujo, C. B. Mendive, L. A. G. Rodenas, P. J. Morando, A. E. Regazzoni, M. A. Blesa and D. Bahnemann, *Colloids and Surfaces A: Physicochemical and Engineering Aspects*, 2005, **265**, 73-80.
30. J. Jasieniak, M. Johnston and E. R. Waclawik, *The Journal of Physical Chemistry B*, 2004, **108**, 12962-12971.
31. L. R. Milgrom, *Journal of the Chemical Society, Perkin Transactions 1*, 1983, DOI: 10.1039/P19830002535, 2535-2539.

32. S. Ito, T. N. Murakami, P. Comte, P. Liska, C. Grätzel, M. K. Nazeeruddin and M. Grätzel, *Thin Solid Films*, 2008, **516**, 4613-4619.
33. M. Späth, P. M. Sommeling, J. A. M. van Roosmalen, H. J. P. Smit, N. P. G. van der Burg, D. R. Mahieu, N. J. Bakker and J. M. Kroon, *Progress in Photovoltaics: Research and Applications*, 2003, **11**, 207-220.
34. A. Stone and E. B. Fleischer, *Journal of the American Chemical Society*, 1968, **90**, 2735-2748.
35. M. Rojkiewicz, P. Kuś, P. Kozub and M. Kempa, *Dyes and Pigments*, 2013, **99**, 627-635.
36. J. P. Lewtak, D. Gryko, D. Bao, E. Sebai, O. Vakuliuk, M. Scigaj and D. T. Gryko, *Organic & Biomolecular Chemistry*, 2011, **9**, 8178-8181.
37. D. A. James, D. P. Arnold and P. G. Parsons, *Photochemistry and photobiology*, 1994, **59**, 441-447.
38. C.-L. Wang, Y.-C. Chang, C.-M. Lan, C.-F. Lo, E. Wei-Guang Diau and C.-Y. Lin, *Energy & Environmental Science*, 2011, **4**, 1788-1795.
39. Y. Ooyama, T. Yamada, T. Fujita, Y. Harima and J. Ohshita, *Journal of Materials Chemistry A*, 2014, **2**, 8500-8511.
40. P. Péchy, T. Renouard, S. M. Zakeeruddin, R. Humphry-Baker, P. Comte, P. Liska, L. Cevey, E. Costa, V. Shklover, L. Spiccia, G. B. Deacon, C. A. Bignozzi and M. Grätzel, *Journal of the American Chemical Society*, 2001, **123**, 1613-1624.
41. F. Nüesch and M. Grätzel, *Chemical Physics*, 1995, **193**, 1-17.
42. Y. Wang, X. Li, B. Liu, W. Wu, W. Zhu and Y. Xie, *RSC Advances*, 2013, DOI: 10.1039/c3ra40788h.
43. A. S. Hart, C. B. Kc, H. B. Gobeze, L. R. Sequeira and F. D'Souza, *ACS Applied Materials & Interfaces*, 2013, **5**, 5314-5323.
44. M. Ameri and E. Mohajerani, *RSC Advances*, 2015.
45. H. Imahori, Y. Matsubara, H. Iijima, T. Umeyama, Y. Matano, S. Ito, M. Niemi, N. V. Tkachenko and H. Lemmetyinen, *The Journal of Physical Chemistry C*, 2010, **114**, 10656-10665.
46. J. H. Delcamp, Y. Shi, J.-H. Yum, T. Sajoto, E. Dell'Orto, S. Barlow, M. K. Nazeeruddin, S. R. Marder and M. Grätzel, *Chemistry – A European Journal*, 2013, **19**, 1819-1827.
47. *Handbook of Photovoltaic Science and Engineering*, second edn.
48. G. Boschloo and A. Hagfeldt, *Accounts of Chemical Research*, 2009, **42**, 1819-1826.

Zinc (II) porphyrins with catechol moiety anchoring group were used in dye sensitized solar cells for the first time.